Parker, I. H. Hutchinson, D. Overskei, and L. S. Scaturro, to be published.
[15]K. L. Wong, P. Bellan, and M. Porkolab, Phys. Rev. Lett., 40, 554 (1978); K. L. Wong, J. R. Wilson, and M. Porkolab, Princeton Plasma Physics Laboratory Report No. PPL-1499, 1979 (unpublished).
[16]L. S. Scaturro and B. Kusse, Nucl. Fusion 18, 1717 (1978).

Electron-Density Structures in Laser-Produced Plasmas at High Irradiances

A. Raven
Rutherford Laboratory, Chilton, Didcot, Oxon, United Kingdom

and

O. Willi
Department of Engineering Science, Oxford University, Oxford, United Kingdom
(Received 26 March 1979)

Interferometric measurements have been made of the electron-density structures produced in plasmas generated by the interaction of 1.06-μm radiation with targets at irradiances I of 10^{16} W cm^{-2}. Strong profile steepening near critical density with an $I^{0.16}$ scaling is observed together with supercritical density bumps and structures attributable to magnetic field effects.

The effects of radiation pressure on the density profiles formed during the interaction of intense laser light with plasmas have been recently reported in the regime where the radiation pressure P_r is a fraction (0.2) of the plasma pressure P_c at critical density.[1] Three types of profile modification have been discussed theoretically[2] of which one type is consistent with numerical studies[3] and favored by stability. In this Letter we present the results of an interferometric study at $\lambda = 266$ nm of the time evolution of density structures produced at irradiances of 10^{16} W cm^{-2} where $P_r > P_c$. Initial steepening of the profile with a step-height scaling of $\Delta n/n_c \propto I^{0.16 \pm 0.01}$ is observed followed by the development at later times of supercritical density structures. A model is proposed for these structures in terms of the plasma flow profiles. Structures are also observed that are attributable to the high magnetic-field pressure ($B^2/8\pi nkT \sim 0.5$) in the low-density corona.

The targets used consisted of small 40-μm-diam hollow glass microballoons or 1-mm-diam aluminum wires. The former were chosen to facilitate probing to high densities.[1] Irradiation of these targets was with a single 50-ps–full-width (at half maximum) pulse of between 0.5 and 2.5 J in a 15-μm focal spot giving irradiances on target of up to 10^{16} W cm^{-2}.

A portion of the main irradiating beam was split off and frequency quadrupled in two successive deuterated potassium dihydrogen phosphate crystals to generate a probe beam at 266 nm. The probe pulse of 150 μJ in 25 ps was used to illuminate the target from the side. Timing with respect to the main beam was to within 15 ps as measured by an EPL streak camera. An $f/2.5$ $\times 10$ ultraviolet microscope objective was used to image the target. Protection of the objective from target debris and scattered 1.06-μm light was achieved by the use of a 100-μm-thick quartz pellicle with a dielectric mirror coating on the front surface. The interferometer was of the Nomarski type[4] and used a quartz Wollaston prism and a calcite Glan-Taylor prism mounted coaxially behind the microscope objective. Interferograms were recorded on Kodak HP5 film. Alignment and focusing were carried out in the He-Ne light with the interference fringes switched off and an empirically determined focal-length correction was then applied to focus the image in 266-nm light. A focal accuracy of 10 μm, which is necessary for the accurate analysis of the density profiles of the strongly refracting plasma,[5] was achieved.

The interferograms were enlarged and fringe-position data were digitized with a computer-linked graphics tablet. Abel inversions[6] were performed along lines normal to the main laser beam and the central values of such inversions, taken every 0.5 μm, were used to obtain the axial (Z) electron-density profiles.

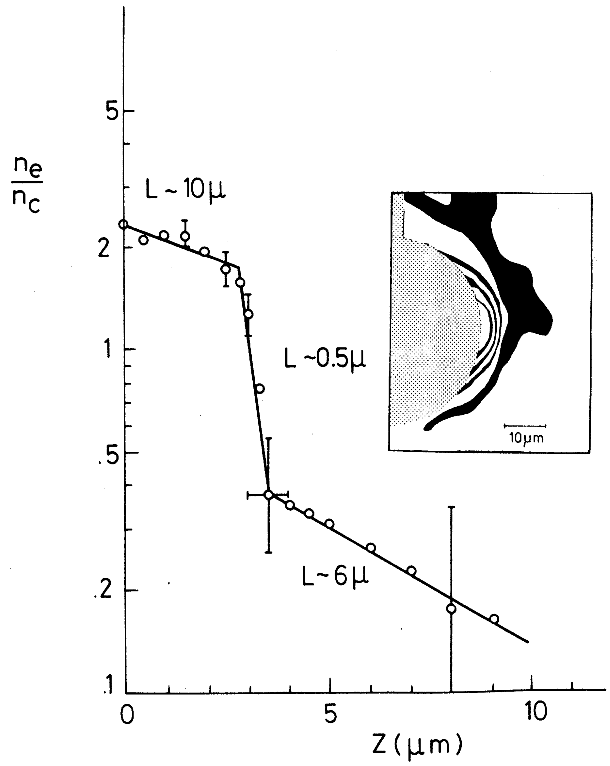

FIG. 1. Radiation-pressure–steepened density profile during the main heating pulse of 10^{16} W cm^{-2} irradiance. Solid lines are best fits to exponentials of the form $e^{-z/L}$. Inset shows the interferogram after computer processing to remove the background fringes.

Measurements on spherical targets during the main heating pulse (Fig. 1) at an intensity of 10^{16} W cm^{-2} show a steepened profile with upper and lower density shelves at $1.8n_c$ and $0.4n_c$, respectively (n_c is the critical density for 1.06 μm $= 10^{21}$ cm^{-3}). The scale length of the steepened section is limited by the optics resolution and plasma motion to 0.5 μm. These results are very similar to those observed by Attwood[1] at the lower intensity of 3×10^{14} W cm^{-2} with the exception that the upper density shelf is, as expected, at a higher density. Measurements made at an intensity of 2.5×10^{15} W cm^{-2} show the step height to be reduced to $1.1n_c$ and these, together with the results of Ref. 1, indicate an intensity scaling of the step height of $\Delta n/n_c = 4.0\times 10^{-3} I^{0.16\pm 0.01}$ with I in W cm^{-2}.

Kidder[7] on the basis of an isothermal plasma with sonic flow through the critical surface has estimated the density step to be proportional to $(P_r/P_c)^{1/2}$ for $P_r/P_c \ll 1$. Numerical work[8] suggests that this half-power law also holds for $P_r/P_c \sim 1$. Experiments[9,10] have shown the electron temperature is related to the incident intensity by $T \propto I^{2/3}$ and consequently the density jump can be estimated to scale as $\Delta n/n_c \propto (I/cnkT)^{1/2} \propto I^{0.17}$. This scaling is in very close agreement with the measured scaling despite the limitations of the theoretical model.

After the main heating pulse a complex density structure develops (Fig. 2). In particular a su-

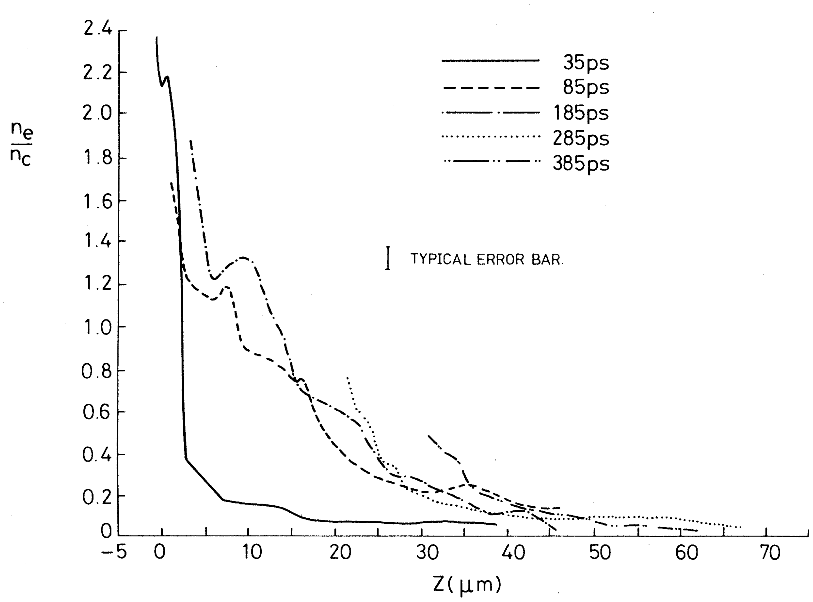

FIG. 2. Time development of electron-density profiles after the main heating pulse of 10^{16} W cm^{-2} irradiance. Profiles at 285 and 385 ps are taken with a second-harmonic probe. Other profiles are with fourth-harmonic probe.

percritical density bump is seen and considerable low-density structure appears. Several shots were taken at each time and all show qualitatively the same density structures. At late times ($t = 285$ ps, 385 ps), the low-density structure relaxes to a smooth two-scale-length profile as has been observed before.[11] The positions of the profiles are referenced with an accuracy of 1 μm to the original target surface and allows the velocity of the critical surface to be determined as $6.3 \pm 0.8 \times 10^6$ cm s^{-1} (Fig. 3). This is consistent with estimates of $V_c \lesssim 5 \times 10^6$ cm s^{-1} obtained from the visibility of the interference fringes and the plasma motion limit on the measured scale length of the steepened profile.

The supercritical density bump in Fig. 2 is similar to the supersonic profile discussed by Max and McKee[2] and numerically modeled by Virmont, Pellat, and Mora.[3] The analysis[2] was carried out for an isothermal plasma with a local momentum deposition at the critical surface due to the light pressure and it led to either a D (step) front for subsonic plasma flow or an R (compression front) for supersonic flow. It was suggested that when driven by light pressure a shock plus D front may be more stable than an R front for supersonic flow. In a laser-produced plasma at high irradiance the incident energy flux due to absorption at or below critical density is greater than can be assimilated by thermal conduction to the more dense plasma. This inward heat flux is further inhibited, e.g., by ion acoustic turbulence and results in the low-density corona thermally decoupling[10,12] from the more dense plasma with a steep temperature step around critical density.[10] Under these conditions the steady-state solutions of Ref. 2 can be remodeled in terms of a nonisothermal plasma (with or without light pressure) and leads to similar flow conditions and density structures that now depend on the temperature ratio α^2 (> 1). When light-pressure effects are omitted, Eqs. (4) and (5) of Ref. 2, now become

$$\frac{\rho_1}{\rho_2} = (1+M_1^2) \pm [(1+M_1^2)^2 - 4M_1^2\alpha^2]^{1/2}/2M_1^2,$$

with

$$M_1 > M_R \equiv \alpha + (\alpha^2-1)^{1/2},$$

or

$$M_1 < M_D \equiv \alpha - (\alpha^2-1)^{1/2},$$

where ρ_1 and M_1 are the upper density and Mach number and ρ_2 is the lower density. The effect of this nonisothermality has been observed in numerical simulations[8] where the D-front density jump was found to be dependent on the flux inhibition factor applied.

After the laser is switched off thermal conduction cooling of the hot corona can be shown to be sufficient to drive ion acoustic turbulence and maintain a temperature step near to critical density for many times the initial laser pulse duration.[13] This temperature step will then maintain a heat wave traveling against the outflow of colder plasma from the target. This heat wave can be of the subsonic (D front) or supersonic (R front) type depending on the local flow conditions. The transition from subsonic to supersonic flow can be induced by lowering the coronal temperature[14] or decreasing the external (e.g., radiation) pressure and will result in the smooth transition from the subsonic radiation plus thermal flux-driven D front during the laser pulse to the supersonic thermal flux-driven R front seen at later times. From an estimate of the local temperature at this time and the magnitude of the density perturbation one can estimate the local power flux to be ~ 3×10^{12} W cm^{-2} which is consistent with the flux-limited heat flow.[13]

Measurements on the wire targets were made 85 ps after the peak of the main heating pulse. At this time strong magnetic fields of order 2 MG have been measured in the low-density (~$0.1c$) co-

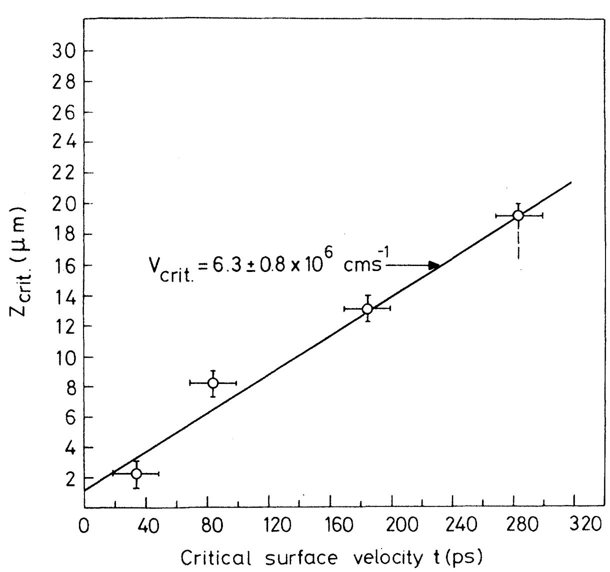

FIG. 3. Critical surface position with time. Position at 285 ps is an extrapolation from the measured profile and represents an upper limit.

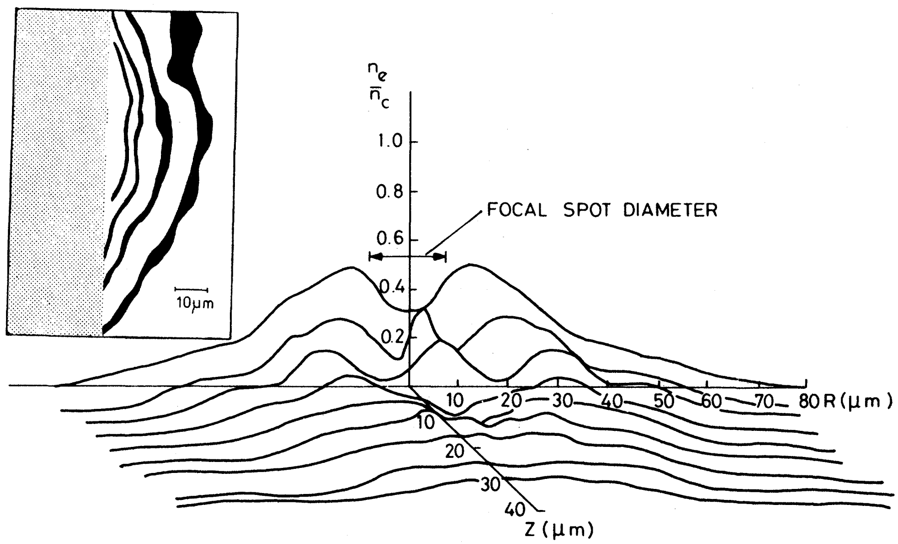

FIG. 4. Density profiles on plane target 85 ps after the peak of the laser pulse. Irradiance is 10^{16} W cm^{-2} and the focal-spot diameter is 15 μm. The off-axis density depression due to the magnetic field pressure is clearly evident on the profiles at $z = 5$ μm and $z = 10$ μm. Inset as in Fig. 1.

rona[6,15] and subsequently been shown to extend to higher densities using a similar fourth-harmonic probing system.[16] A typical density profile at an intensity of 10^{16} W cm^{-2} is shown in Fig. 4. The profile at high density shows the familiar hollowing by the incident radiation pressure to a half-width equal to the focal spot radius, and a density minimum equal to that of the lower shelf density on spherical targets. In lower-density plasma this changes to a double hollow structure with minima off axis at the focal spot radius. This correlates well with the measured position of the magnetic fields.[6,16] The field pressure in this low-density region can be estimated at approximately 50% of the thermal pressure of the plasma in agreement with the observed 50% depletion of the local plasma density. At still lower densities, this profile reverts to the low-density shell-type structure measured previously[6] that rings the field region. The role of the magnetic field in pushing the plasma out into a shell structure and creating an on-axis density maximum is clearly evident. The profiles measured on the spherical targets showed no such structures and are further evidence for no significant fields on this type of target.[6,16]

In conclusion we have presented measurements of electron-density profiles at high irradiance and demonstrated the effects of both radiation and magnetic-field pressure on the plasma. The scaling of step height with intensity has been measured and the transition from a D-front- to an R-front-type structure has been observed. A model for this transition has been proposed involving heat-wave propagation in a nonisothermal supersonic plasma.

The authors would like to thank B. Ahlborn and P. T. Rumsby for helpful discussions, and acknowledge the support of the Rutherford Laboratory Laser Division staff.

[1]D. T. Attwood *et al.*, Phys. Rev. Lett. 40, 184 (1978).
[2]C. E. Max and C. F. McKee, Phys. Rev. Lett. 39, 1336 (1977).
[3]J. Virmont, R. Pellat, and A. Mora, Phys. Fluids 21, 567 (1978); K. A. Brueckner and R. S. Janda, Nucl. Fusion 17, 451 (1977).
[4]R. Benattar, C. Popovics, and R. Sigel, "A polarised light interferometer for laser fusion studies" (unpublished).
[5]C. M. Vest, Appl. Opt. 14, 1601 (1975).
[6]A. Raven, O. Willi, and P. T. Rumsby, Phys. Rev. Lett. 41, 554 (1978); and J. Stamper, U. S. Naval Research Laboratory Report No. 3872, 1978 (unpublished).
[7]R. E. Kidder, in Proceedings of Japan–U. S. Seminar on Laser Interaction with matter, Tokyo, 1975 (unpublished).
[8]J. T. Larsen and J. Harte, Bull. Am. Phys. Soc. 20, 1061 (1977).
[9]N. Minyanaga and K. Tanaka, Osaka University Report No. ILE-APR-77, 1977 (unpublished).
[10]M. D. Rosen *et al.*, Lawrence Livermore Laboratory Report No. UCRL-82146, 1978 (unpublished); P. M. Campbell *et al.*, Phys. Rev. Lett. 39, 274 (1977); R. C. Malone, R. L. McCrory, and R. L. Morse, Phys. Rev.

Lett. 34, 721 (1975).
[11]H. Azechi *et al.*, Phys. Rev. Lett. 39, 1144 (1977).
[12]R. E. Kidder and J. W. Zink, Nucl. Fusion 12, 1325 (1972).
[13]A. Raven and B. Ahlborn, Rutherford Laboratory Laser Division Report No. LD/79/01, 1979 (unpublished).
[14]B. Ahlborn and S. Ariga, Phys. Fluids 20, 18 (1977).
[15]J. A. Stamper, E. A. McLean, and B. H. Ripin, Phys. Rev. Lett. 40, 1177 (1978).
[16]A. Raven *et al.*, to be published.

Computer Simulation of the Time Evolution of a Quenched Model Alloy in the Nucleation Region

J. Marro[(a)]
Departamento de Física Teórica, Universidad de Barcelona, Barcelona 28, Spain

and

Joel L. Lebowitz
Department of Mathematics and Physics, Rutgers College, New Brunswick, New Jersey 08903

and

M. H. Kalos
Courant Institute of Mathematical Sciences, New York University, New York, New York 10012
(Received 2 January 1979)

The time evolution of the structure function and of the cluster (or grain) distribution following quenching in a model binary alloy with a small concentration of minority atoms is obtained from computer simulations. The structure function $\bar{S}(k,t)$ obeys a simple scaling relation, $\bar{S}(k,t)=K^{-3}F(k/K)$ with $K(t)\propto t^{-a}$, $a\cong 0.25$, during the latter and larger part of the evolution. During the same period, the mean cluster size grows approximately linearly with time.

The process of segregation (nucleation, spinodal decomposition, coarsening, and Ostwald ripening) in alloys following quenching from the melt into the miscibility gap (a common situation in practice) determines many properties of the alloy and is, therefore, of great importance. The theoretical analysis of this problem is based mainly on the classical works of Cahn and Hilliard[1] and of Lifshitz and Slyozov.[2] The former work, as formulated by Cook,[3] describes the evolution of the structure function $S(k,t)$ while the latter considers the grain distribution $n(l,t)$, where t is the time since quenching, k is a reciprocal wave vector, and l is a grain size. This division corresponds[3] directly to the two principal experimental methods of study: x-ray (or neutron) scattering for $S(k,t)$ and electron microscopy for $n(l,t)$.

These classic works have been the subject of considerable study, criticism, extension, etc., in recent years. In particular, the work of Langer, Bar-on, and Miller[4] and Binder and coworkers[5] focusing, respectively, on the structure function and on grain (droplet, cluster) formation and aggregation has been of great importance. These studies have made use of controlled computer experiments of this process in simple model systems carried out by the authors[6] (and others). We now report a striking new feature found in recent computer simulations. This goes qualitatively beyond previous results and deserves, we believe, the attention of both theoreticians and experimentalists. Our results indicate that at low temperatures, $T\simeq 0.6T_c$, and small fractional concentration of A atoms, $\rho=0.075$ and 0.1 (compared to 0.015 on the coexistence line), the time evolution of the model system has the following features for large t:
(1) The normalized structure function $\bar{S}(k,t)$ [see Eq. (9)] can be represented by a simple scaling form[2] $\bar{S}(k,t)=[K(t)]^{-3}F(k/K(t))$ with $K(t)\propto t^{-a}$ and $a\simeq 0.25$. (2) The average cluster size increases approximately linearly with time, $\langle l\rangle \simeq a_0+t/\tau$, in agreement with the Lifshitz-Slyozov[2] theory.

Our model consists of the following: At each site of a simple-cubic lattice of $N=125\,000$ sites with periodic boundary conditions, there is either an A atom or a B atom[6]; the variable $\eta(\vec{r}_i)$ takes on the values $+1$ (-1) when there is an A (B)

